On the Assignment and Directional Dispersion of Polar Phonon Modes in $K_3Cu(CN)_4$ and $K_3Ag(CN)_4$

W. Nitsch, H. J. Falge, and R. Claus

Sektion Physik der Universität München, Lehrstuhl J. Brandmüller, München, Germany

(Z. Naturforsch. **29 a**, 1011–1016 [1974]; received April 25, 1974)

Polar phonon modes in single crystalline $K_3Cu(CN)_4$ and $K_3Ag(CN)_4$ have been experimentally studied by light scattering. Measurements at 293, 82 and 6 K made possible assignments in the low frequency region from 0 to about 700 cm^{-1} and the high frequency region from 2030 to about 2100 cm^{-1} originating from the C≡N stretching vibrations. Directional dispersion due to the anisotropy of $K_3Cu(CN)_4$ has been studied and allowed the identification of the transversal and longitudinal vibrations in the high frequency region. IR-reflectivity measurements, partly on the basis of the ATR-method, have been used in order to support the assignments in this region.

Introduction

First crystallographic investigations concerning the structure of $K_3Cu(CN)_4$ have been published by Cox, Wardlaw and Webster in 1936 [1] and Staritzky and Ellinger in 1956 [2]. The material was found to belong to the space group R 32 ($=D_3^7$). In 1966 and 1967, however, Giusepetti and Tadini [3] and Haussühl [4], respectively, could unambigously determine the material to be hexagonal of the crystal class 3 m ($=C_{3v}$). Finally in 1968 Roof, Larson and Cromer [5] published extensive investigations concerning the crystal structure leading to the space group R 3 c ($=C^6_{3v}$). These authors presented detailed crystallographic data which have been used in the present work. The crystal is built up by K^+-ions and $Cu(CN)_4^{3-}$-tetrahedrons. The six nearest neighbours of a potassium ion are N-atoms or CN-groups belonging to five different $Cu(CN)_4^{3-}$-tetrahedrons. These neighbours build up a slightly distorted octahedron. The unit cell consists of two molecules.

$K_3Ag(CN)_4$ is isomorphous to $K_3Cu(CN)_4$. The only paper concerning the structure of this material was published 1956 by Staritzky and Ellinger [6]. In analogy to their work on $K_3Cu(CN)_4$ they report the space group R 32 ($=D_3^7$). However, there seems to be no doubt that also $K_3Ag(CN)_4$ belongs to the space group R 3 c ($=C^6_{3v}$). Factor group analysis in the way reported by Behringer [7] leads to Table I when using the data from Reference [5]. The A_2-modes are neither IR – nor Raman-active and thus silent whereas the A_1 and E modes are IR – as well as Raman-active. Both types of phonons are expected to show polariton dispersion which is observable by light scattering. If the translations representing the acoustical branches are omitted there should be 11 optical phonons of type A_1 and 23 of type E. For wave vector directions in the optically isotropic plane there will simultaneously be ordinary E (TO)-modes and extraordinary E (LO)-modes. Because of the frequency splitting described by the Lyddane-Sachs-Teller relation [8] a maximum number of polar E-modes = 46 is expected in this case whereas in direction of the optic axis (z) the extraordinary E (TO)-modes degenerate with the ordinary. The number of A_1-phonons will be 11 for both wave vector directions ($\boldsymbol{k}$). The frequencies, however, will be those of A_1 (TO)-modes for $\boldsymbol{k} \perp z$ and those of A_1 (LO)-modes for $\boldsymbol{k} \parallel z$. These discrepancies with Table 1 appear because the Raman scattering experiments are carried out for phonon wave vectors of the order $k \approx 10^5$ cm^{-1} whereas the prediction of group theory is valid for $k = 0$ only, see for instance [9].

Tab. 1. Factor group analysis of $K_3Cu(CN)_4$.

	Translations	Translational vibrations	Librations	Internal vibrations	IR-activity	Raman-activity
A_1	1	3	1	7	yes	yes
A_2	0	4	1	7	no	no
E	1	7	2	14	yes	yes

Experimental Results

The phonon spectrum of $K_3Cu(CN)_4$ has previously been studied by Poulet and Mathieu [10] and Claus [11]. Because of strong damping most of the Raman lines have great half band widths and thus especially in the low frequency region it was impos-

sible to resolve all Raman lines at room temperature. Therefore in the present work the material has been studied also at 82 K and 6 K. Figure 1 shows the phonons of A_1-type in the lower frequency region recorded using the scattering geometry $x\ (z\,z)\,y$. The

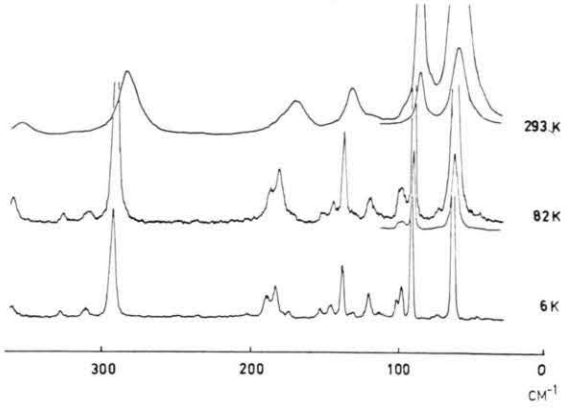

Fig. 1. A_1-type phonons in $K_3Cu(CN)_4$ recorded using the scattering geometry $x(zz)y$. Exciting line = 514,5 nm, laser output = 1 W, spectral slit width = 2 cm^{-1}. The spectra are recorded at 293, 82 and 6 K, respectively.

scattering triangles $\boldsymbol{k}_i = \boldsymbol{k}_s + \boldsymbol{k}$ were restricted to lie parallel to the optically isotropic plane $(x\,y)$. $\boldsymbol{k}_i$ and $\boldsymbol{k}_s$ denote the wave vectors of the incident and scattered photons, respectively. The frequencies therefore are those of exactly transversal phonons. Figure 2 shows the corresponding spectra of E-type

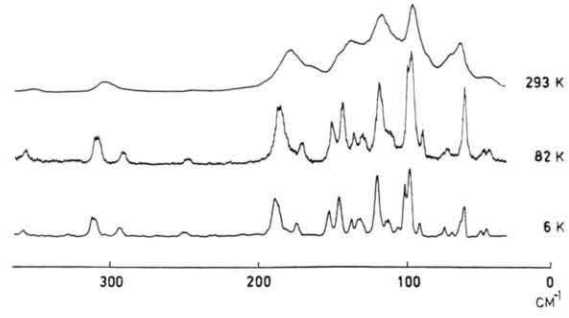

Fig. 2. E-type phonons in $K_3Cu(CN)_4$ recorded using the scattering geometry $y(xz)x$. Exciting line = 514,5 nm, laser output = 1 W, spectral slit width = 2 cm^{-1}. The spectra are recorded at 293, 82 and 6 K, respectively.

phonons observed by the scattering geometry $y(x\,z)x$. In these spectra both TO and LO-modes are expected. Directional dispersion measurements with phonon wave vectors forming different angles with the optic axis showed that the anisotropy in most cases causes TO – LO splittings in the region to about 700 cm^{-1} which are hardly observable at room temperature.

Figure 3 shows the high frequency spectra which are caused by the C ≡ N stretching vibrations. α_{zz}-scattering shows two strong modes of A_1-type at 2093.5 and 2074 cm^{-1} and two modes which are about a factor 64 weaker at 2046 and 2032.5 cm^{-1}.

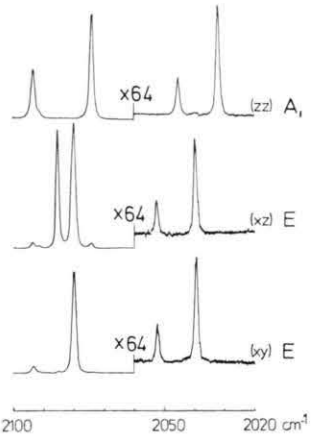

Fig. 3. High frequency phonon spectrum of $K_3Cu(CN)_4$ caused by C≡N vibrations, see text.

Scattering due to the non diagonal elements of the Raman tensor on the other hand allows the identification of two strong phonons of E-type at 2085 and 2080 cm^{-1} and again two weak modes at 2053 and 2040 cm^{-1}. Extensive investigations by Nitsch and Claus [12] unambigously showed that the four weak phonons are caused by vibrations of the isotopes ^{13}C and ^{15}N against their neighbours ^{14}N and ^{12}C, respectively. The strong phonons on the other hand are fundamentals. From the general polariton theory [13] follows that the directional dispersion of extraordinary phonons is given by

$$\mathrm{tg}^2\,\Theta = -\varepsilon_{\parallel}(\omega)/\varepsilon_{\perp}(\omega)\ . \tag{1}$$

Herein Θ denotes the angle between the phonon wave vector and the optic axis. $\varepsilon_{\parallel}(\omega)$ and $\varepsilon_{\perp}(\omega)$ are the frequency dependent dielectric constants for directions parallel and perpendicular to the optic axis, respectively. Explicitely these are given by

$$\varepsilon_{\parallel}(\omega) = \varepsilon_{\parallel\infty} \prod_{i=1}^{m} \frac{\omega_{\parallel iL}^2 - \omega^2}{\omega_{\parallel iT}^2 - \omega^2}\ , \tag{2}$$

and

$$\varepsilon_{\perp}(\omega) = \varepsilon_{\perp\infty} \prod_{j=1}^{m_\perp} \frac{\omega_{\perp jL}^2 - \omega^2}{\omega_{\perp jT}^2 - \omega^2}\ , \tag{3}$$

where $\varepsilon_{\parallel\infty}$ and $\varepsilon_{\perp\infty}$ are the corresponding dielectric constants for frequencies which are great compared

with those of the phonons in the reststrahlen band region. $\omega_{\parallel iL}$ and $\omega_{\parallel iT}$ are the frequencies of the A(LO) and A(TO)-modes whereas $\omega_{\perp jL}$ and $\omega_{\perp jT}$ are those of E(LO) and E(TO) modes, respectively. In $K_3Cu(CN)_4$ the high frequency region is well separated from the low frequency region by a gap of more than 1300 cm^{-1} where no first order phonons are expected. This suggests us to treat the C ≡ N vibrations as isolated since they are only very weakly coupled to the other modes. Directional dispersion measurements will allow the determination of all first order TO and LO-modes in this region. Experimental results are reproduced in Figure 4. The angle Θ between the optic axis and

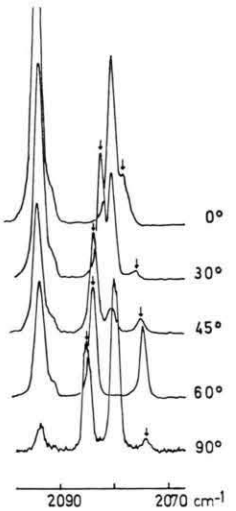

Fig. 4. Directional dispersion of extraordinary phonon modes in the high frequency region corresponding to C≡N vibrations of $K_3Cu(CN)_4$. The angles to the right denote that between the wave vector and the optic axis.

the wave vector is given to the right, $\Theta = 0$ corresponding to $\boldsymbol{k} \parallel z$ and $\Theta = 90^\circ$ to $\boldsymbol{k} \perp z$. For decreasing Θ from $\pi/2$ to 0 the A_1(TO)-phonon does hardly show any frequency shift. The E-phonon at 2085 on the other hand is shifted to 2080 cm^{-1} for $\Theta = 0^\circ$ which obviously corresponds to an E(TO)-phonon. The A_1(TO)-phonon at 2074 cm^{-1} correspondingly is shifted to 2077 cm^{-1} and will here be longitudinal of type A_1 because $\boldsymbol{k} \parallel z$. The relations (2) and (3) require that the lowest frequency phonon will be transversal whereas the highest frequency phonon of the group necessarily has to be an LO-mode. Furthermore for both A_1 and E-modes the phonon sequence for increasing wave numbers has to be TO, LO, TO, LO etc. because between two poles of the dielectric function $\varepsilon(\omega)$ the function has to assume the value $\varepsilon(\omega) = 0$ once. The zeros of the dielectric functions, however, determine the frequencies of the LO-modes: $\omega = \omega_{\parallel iL}$ and $\omega = \omega_{\perp jL}$ whereas the poles determine those of TO-phonons: $\omega = \omega_{\parallel iT}$ and $\omega_{\perp jT}$ as can immediately by seen from Eqs. (2) and (3), respectively. Accordingly the phonon at 2085 cm^{-1} will be longitudinal of type E and the LO-mode corresponding to the A_1(TO)-phonon at 2093 cm^{-1} is expected at almost the same frequency. Raman scattering experiments did not allow the observation of this TO − LO-splitting. We therefore made IR-reflectivity measurements using the ATR-method in order to ensure the assignment, see [14]. These experiments suggested the wave number 2094 cm^{-1} for the A_1(LO)-phonon. The results are reproduced in Figures 6 and 7.

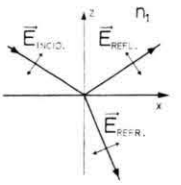

Fig. 5. Incident ($\boldsymbol{E}_{\text{incid}}$), reflected ($\boldsymbol{E}_{\text{refl}}$) and refracted ($\boldsymbol{E}_{\text{refr}}$) ray when using TH-reflection, see text.

The principle of the experiment can be seen from Fig. 5. An incident electromagnetic wave ($\boldsymbol{E}_{\text{incid}}$) is partly reflected ($\boldsymbol{E}_{\text{refl}}$) and partly refracted ($\boldsymbol{E}_{\text{refr}}$) by the surface of a crystalline medium. The optic axis z of the crystal stands vertically to the surface. $\boldsymbol{E}_{\text{refr}}$ then corresponds to the extraordinary ray in the material. The upper medium with the refractive index n_1, is isotropic. All light waves are polarized in the figure plane i.e. the magnetic polarization stands perpendicularly to the optic axis and the figure plane. This has become known as transverse magnetic polarization (TH-polarization). The reflectivity is then given by

$$R_{\text{TH}}(\omega, \alpha) = \left| \frac{\sqrt{\varepsilon_x}\sqrt{\varepsilon_z}\,\frac{\omega}{c}\cos\alpha - n_1\sqrt{\varepsilon_z\frac{\omega^2}{c^2} - k_x^2}}{\sqrt{\varepsilon_x}\sqrt{\varepsilon_z}\,\frac{\omega}{c}\cos\alpha + n_1\sqrt{\varepsilon_z\frac{\omega^2}{c^2} - k_x^2}} \right|^2 . \tag{4}$$

α refers to $\sphericalangle(E_{\text{incid}}, z)$.

For extraordinary bulk polaritons with wave vectors $\boldsymbol{k}_{\text{BP}}$ propagating perpendicularly to the optic axis (in x-direction of Fig. 5) holds

$$\varepsilon_z = c^2 k_{\text{BP}}^2/\omega^2 . \tag{5}$$

Equation (4) then becomes

$$R_{TH}(\omega, \alpha) = \left| \frac{\sqrt{\varepsilon_x}\, k_{BP} \cos\alpha - n_1 \sqrt{k_{BP}^2 - k^2}}{\sqrt{\varepsilon_x}\, k_{BP} \cos\alpha + n_1 \sqrt{k_{BP}^2 - k^2}} \right|^2 . \quad (6)$$

Because the $\boldsymbol{k}_x$-component of $\boldsymbol{E}_{refr}$ propagates parallel to $\boldsymbol{K}_{BP}$ we simply wrote $k_x = k$. Total reflection appears if one but not both of the terms in (4) and (6) become imaginary. This happens for $\varepsilon_z > 0$ when either ε_x or $(\boldsymbol{k}^2_{BP} - \boldsymbol{k}^2)$ becomes negative and for $\varepsilon_z < 0$, $\varepsilon_x < 0$ is required [14]. The corresponding regions in the high frequency polariton dispersion diagram of $K_3Cu(CN)_4$ have been hatched in Figure 6 a. In all other cases we have reduced reflectivity associated with a real $\boldsymbol{k}$-component of the refracted ray ($\boldsymbol{E}_{refr}$) in z-direction

$$k_z = \frac{1}{\varepsilon_z} \sqrt{\left(\varepsilon_z \frac{\omega^2}{c^2} - k_x^2\right) \varepsilon_x \varepsilon_z} = \frac{1}{\varepsilon_z} \sqrt{(k_{BP}^2 - k^2)\, \varepsilon_x \varepsilon_z} . \quad (7)$$

This wave couples with the optical phonons propagating in z-direction. According to Eq. (7) the limiting curves separating the regions of total and reduced reflection are identical to the dispersion curves of polaritons propagating parallel to the surface (in x-direction) with lattice displacements perpendicular to the surface (in z-direction). Recording the IR-reflection or ATR spectrum for a fixed angle $\alpha = \alpha_0$ then leads to scans $R = R_{TH}(\omega, \alpha_0)$ as indicated for $\alpha = 24°$ and $\alpha = 32°$ in Figure 6 a. The corresponding spectra are reproduced in Figures 6 b and c.

Figure 7 correspondingly shows the ordinary polaritons of the frequency region in question. The

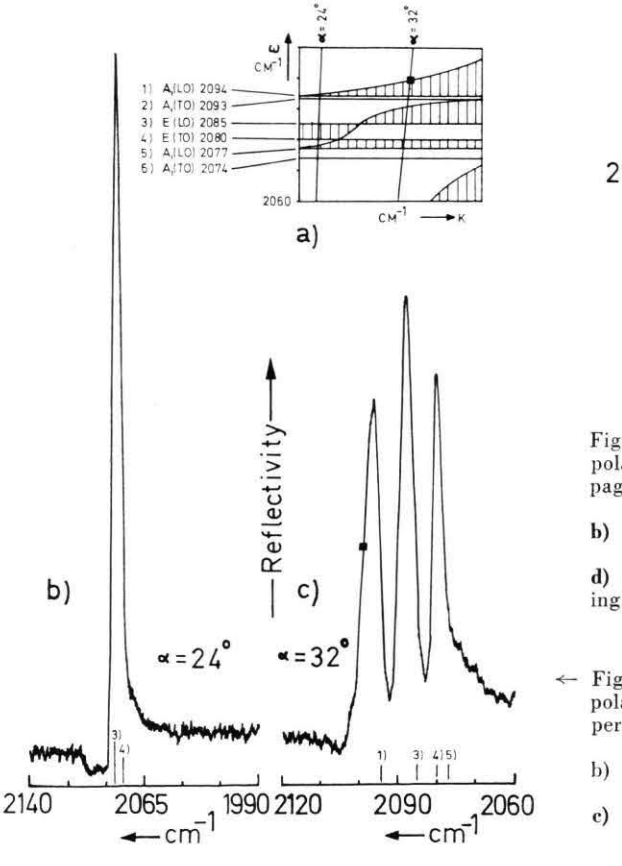

← Fig. 6. **a)** ω-k-diagram of the high frequency extraordinary polariton spectrum of $K_3Cu(CN)_4$ for wave vector directions perpendicular to the optic axis, see Fig. 5. Regions with total reflection have been hatched.
b) IR-reflection scan corresponding to $\alpha = 24°$ as indicated in a).
c) ATR-reflection-spectrum (n_1: KRS 5) corresponding to $\alpha = 32°$ as indicated in a).

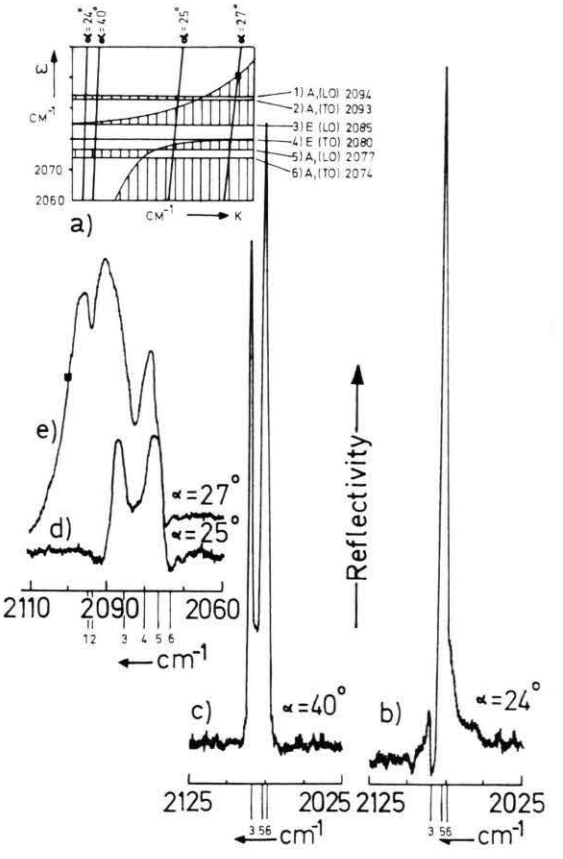

Fig. 7. **a)** ω-k-diagram of the high frequency ordinary polariton spectrum of $K_3Cu(CN)_4$ for wave vectors propagating parallel to the optic axis, see text. Regions with total reflection have been hatched.
b) and **c)** IR-reflection scans corresponding to $\alpha = 24°$ and $\alpha = 40°$, respectively, as indicated in a).
d) and **e)** ATR-reflection-spectra (n_1: KRS 5) corresponding to $\alpha = 25°$ and $\alpha = 27°$, respectively, as indicated in a).

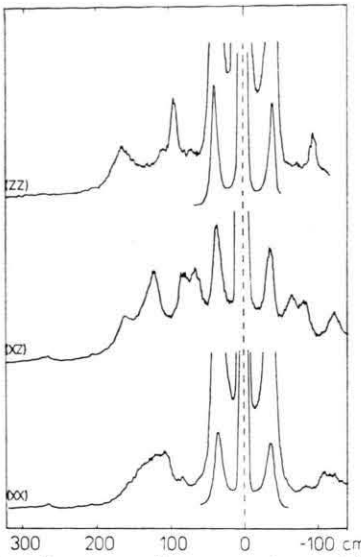

Fig. 8. Low frequency phonon spectrum of $K_3Ag(CN)_4$. α_{zz}-scan showing A_1-type phonons, α_{xz}- und α_{xx}-scans showing E-type phonons. Laser line 647,1 nm, 600 mW. Spectral slit width: 2 cm^{-1}.

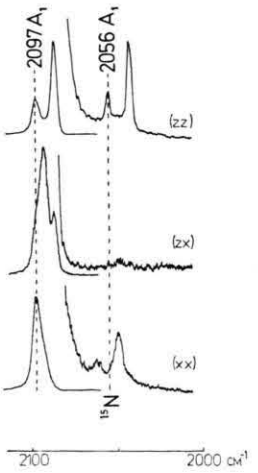

Fig. 9. High frequency phonon spectrum of $K_3Ag(CN)_4$ originating from C≡N stretching vibrations, see data of Figure 8.

experiments have been carried out in the same way as indicated in Figure 5. Only the optic axis (z) was parallel to the surface and $\boldsymbol{k}_x$.

We finally report some results concerning $K_3Ag(CN)_4$. The low and high frequency phonon spectra are shown in Figures 8 and 9. The material is isomorphous to $K_3Cu(CN)_4$ belonging to the space group R 3 c ($=C_{3v}^6$). In contrast to this material $K_3Ag(CN)_4$ is extremely sensitive to temperature gradients and the atmosphere. This prevented detailed investigations as directional dispersion measurements. The results may, however, support the interpretation of the phonon spectra of $K_3Cu(CN)_4$. Especially it should be pointed out that also in this material modes originating from isotopic impurities due to ^{13}C and ^{15}N have been recorded and identified in the high frequency spectrum. The results concerning both materials have been collected in Table 2.

Tab. 2. Wave numbers and assignments of phonon modes in $K_3Cu(CN)_4$ recorded at He-temperatures and $K_3Ag(CN)_4$ at room temperature.

$K_3Cu(CN)_4$		$K_3Ag(CN)_4$	
Wave number	Assignment	Wave number	Assignment
46	E (TO)	35	E
49	E (LO)	38	A_1
61	E?	64	E
63	A_1	80	E
69	E	94	A_1
74	E	120	E
91	A_1	155 ± 5	E
98	E	163	A_1
102	E	199	E
107	E	262	E
113	E		
121	E		
133	E		
139	A_1		
147	E		
153	E		
174	E		
183	A_1		
189	E		
245	A_1		
250	E		
294	A_1		
311	E		
313	E		
329	A_1		
360	E		
363	A_1		
372	E		
607	A_1		
619	A_1?		
627	A_1?		
2032,5	A_1 $^{13}C{\equiv}N$	2043,5	A_1 $^{13}C{\equiv}N$
2040	E $^{13}C{\equiv}N$	2051	E $^{13}C{\equiv}N$
2046	A_1 $C{\equiv}^{15}N$	2056	A_1 $C{\equiv}^{15}N$
2053	E $C{\equiv}^{15}N$	2064	E $C{\equiv}^{15}N$
2074	A_1 (TO)	2088	A_1
2077	A_1 (LO)		
2080	E (TO)	2093	E
2085	E (LO)		
2093	A_1 (TO)	2097	A_1
2094	A_1 (LO)		

Acknowledgements

We thank Prof. S. Haussühl for providing excellent crystal samples of both materials and Prof. J. Brandmüller for discussions and his active interest. The work was financially supported by the Deutsche Forschungsgemeinschaft.

[1] E. G. Cox, W. Wardlaw, and K. Webster, J. Chem. Soc. **125**, 775 [1936].
[2] E. Staritzky and F. H. Ellinger, Analyt. Chem. **28**, 422 [1956].
[3] G. Giusepetti and C. Tadini, Per. Mineral. **35**, 431 [1966].
[4] S. Haussühl, Z. Kristallogr. **125**, 1 [1967].
[5] R. B. Roof, A. C. Larson, and D. T. Cromer, Acta Cryst. **B 24**, 269 [1968].
[6] E. Staritzky and F. H. Ellinger, Analyt. Chem. **28**, 423 [1956].
[7] J. Behringer, Factor Group Analysis Revisited and Unified, Springer-Verlag, Berlin, Tracts Mod. Phys. **68**, 161 [1973].
[8] M. Born and K. Huang, Dynamical Theory of Crystal, Lattices, Clarendon Press, Oxford 1966.
[9] R. Claus, Phys. Stat. Sol. (b) **50**, 11 [1972].
[10] H. Poulet and J. P. Mathieu, Spectrochim. Acta **11**, 932 [1959].
[11] R. Claus, Thesis, Munich 1970.
[12] W. Nitsch and R. Claus, Z. Naturforsch. **29 a**, 1017 [1974]; nachstehende Arbeit.
[13] L. Merten, Festkörperprobleme XII, Advances in Solid State Physics, Vieweg Pergamon 1972, p. 343 ff.
[14] H. J. Falge, A. Otto, and W. Sohler, Phys. Stat. Sol. (b) **63**, 259 [1974].
[15] H. J. Falge, Thesis, Munich 1974.